JCB Journal of Cell Biology

REPORT

Architecture of the cortical actomyosin network driving apical constriction in *C. elegans*

Pu Zhang[1*], Taylor N. Medwig-Kinney[1*], and Bob Goldstein[1,2]

Apical constriction is a cell shape change that drives key morphogenetic events during development, including gastrulation and neural tube formation. The forces driving apical constriction are primarily generated through the contraction of apicolateral and/or medioapical actomyosin networks. In the *Drosophila* ventral furrow, the medioapical actomyosin network has a sarcomere-like architecture, with radially polarized actin filaments and centrally enriched non-muscle myosin II and myosin activating kinase. To determine if this is a broadly conserved actin architecture driving apical constriction, we examined actomyosin architecture during *C. elegans* gastrulation, in which two endodermal precursor cells internalize from the surface of the embryo. Quantification of protein localization showed that neither the non-muscle myosin II NMY-2 nor the myosin-activating kinase MRCK-1 is enriched at the center of the apex. Further, visualization of barbed- and pointed-end capping proteins revealed that actin filaments do not exhibit radial polarization at the apex. Our results demonstrate that *C. elegans* endodermal precursor cells apically constrict using a mixed-polarity actin filament network and with myosin and a myosin activator distributed throughout the network. Taken together with observations made in other organisms, our results demonstrate that diverse actomyosin architectures are used in animal cells to accomplish apical constriction.

Introduction

During development, tissues are remodeled through morphogenesis, which is largely driven by forces generated at the level of individual cells. One of the strategies utilized to achieve morphogenesis is apical constriction (Fig. 1 A). Apical constriction is essential for several morphogenetic events, including gastrulation in many organisms such as *Drosophila* and *Caenorhabditis elegans* and neural tube formation in vertebrates (reviewed in Sawyer et al., 2010). Apical constriction is primarily driven by the contraction of actomyosin networks at the apical cortex, where non-muscle myosin II motor proteins pull on actin filaments, generating cortical tension (reviewed in Martin and Goldstein, 2014).

Several models have been proposed for the organization of actomyosin networks in apically constricting cells (Fig. 1 B; reviewed in Martin and Goldstein, 2014). One of the earliest described models is the circumferential contraction network or "purse string" model, which has been thought to drive apical constriction in vertebrates (Baker and Schroeder, 1967; Burnside, 1973). In this model, actin filaments and non-muscle myosin II are enriched at the periphery of the cell apex and generate pulling forces parallel to apicolateral junctions. Another model is the medioapical contractile model, in which the actomyosin network spans the cell apex and generates pulling forces largely perpendicular to apicolateral junctions (Martin and Goldstein, 2014).

The medioapical actomyosin network driving apical constriction of epithelial cells in the ventral furrow of *Drosophila* exhibits a radial sarcomere-like pattern (Coravos and Martin, 2016). In this context, actin filaments are polarized with barbed ends enriched apicolaterally and pointed ends enriched toward the center of the apex, where myosin and the myosin-activating kinase ROCK are also enriched (Coravos and Martin, 2016; Martin et al., 2009; Mason et al., 2013). The enrichment of ROCK in the center of the apex appears to be important in this system because mislocalizing active ROCK broadly across the medioapical cortex disrupted apical constriction (Coravos and Martin, 2016). This work with the *Drosophila* ventral furrow is the first to quantify the orientation of actin filaments together with the precise distributions of myosin and a myosin activator in apically constricting cells. Thus, it remains unclear to what extent other medioapical actomyosin networks that drive apical constriction share aspects of this radial sarcomere-like organization.

[1]Biology Department, University of North Carolina at Chapel Hill, Chapel Hill, NC, USA; [2]Lineberger Comprehensive Cancer Center, University of North Carolina at Chapel Hill, Chapel Hill, NC, USA.

*P. Zhang and T.N. Medwig-Kinney contributed equally to this paper. Correspondence to Bob Goldstein: bobg@unc.edu.

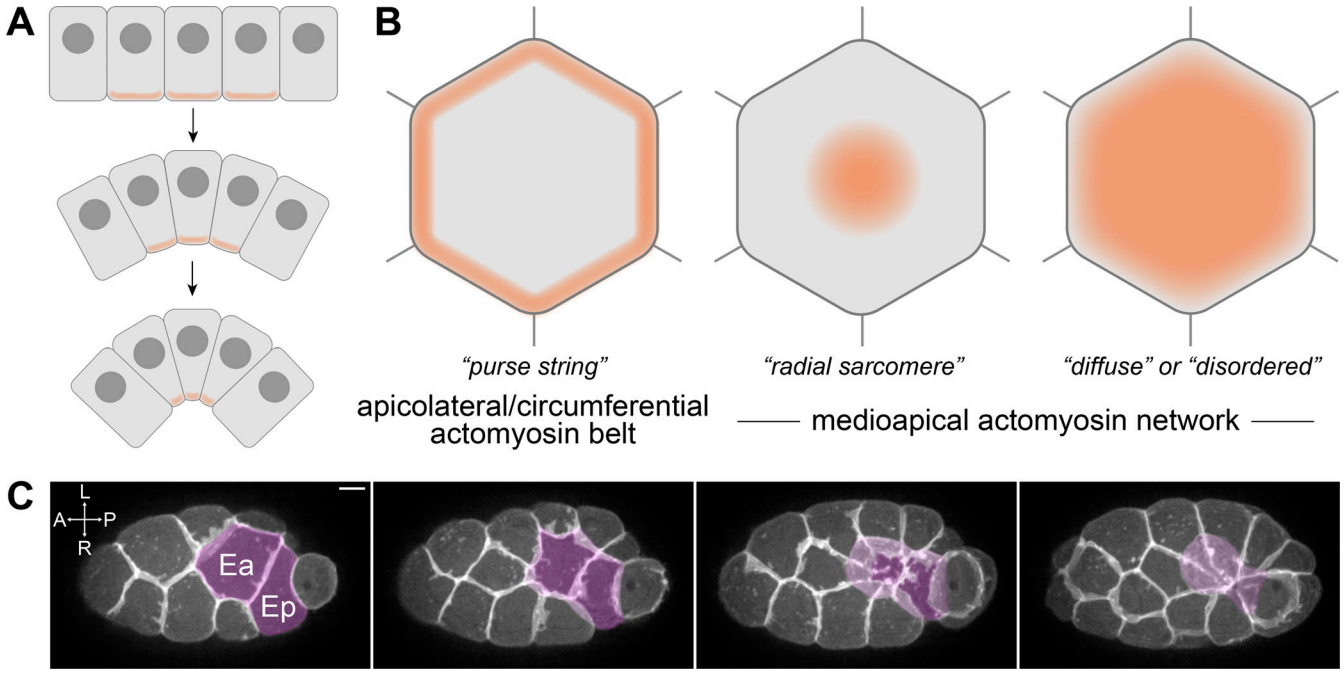

Figure 1. **Models of apical constriction. (A)** Illustration of apical constriction resulting in tissue morphogenesis. **(B)** Three of the models of actomyosin architecture observed in apically constricting cells. Orange shading represents the regions of localized myosin-based force generation. **(C)** Maximum-intensity projections of 10 planes spanning 5 µm total Z-depth depicting *C. elegans* gastrulation from a ventral view with plasma membranes fluorescently labeled (*mex-5p*::mScarlet-I::PH). Ea and Ep are pseudocolored to visualize their internalization over time. L, R, A, and P indicate left, right, anterior, and posterior, respectively. Scale bar: 5 µm.

To determine if a radially polarized medioapical actomyosin network is a broadly conserved architecture during apical constriction, we examined actomyosin dynamics during *C. elegans* gastrulation. Gastrulation in *C. elegans* begins with the internalization of the endodermal precursor cells Ea and Ep into the embryo at the 26–28-cell stage (Fig. 1 C). This model of apical constriction is valuable for examining precise actomyosin architecture due to its amenability for live-cell imaging, its well-defined and stereotyped set of cells involved, and conserved cell behaviors (Goldstein and Nance, 2020). We used live-cell imaging of endogenously tagged proteins and quantification of protein localization to resolve the actomyosin architecture of apically constricting cells. Considering that the distribution of key proteins and orientation of actin filaments might mirror those found in *Drosophila* ventral furrow cells strongly, weakly, or not at all, we considered it important to quantitatively analyze protein localization. We report that the non-muscle myosin II NMY-2 and myosin-activating kinase MRCK-1 are not enriched at the center of the cell apex, but instead exhibit punctate distribution throughout the cell apex. Additionally, we generated reagents to visualize the polarization of actin filaments. We report that the barbed-end actin filament capping protein CAP-1 is enriched at cell–cell contacts, but the pointed-end actin filament capping protein UNC-94 is distributed throughout the cell apex, suggesting that actin filaments are not radially polarized in this system as they are in *Drosophila* ventral furrow cells but rather are more diffusely organized.

Results and discussion

NMY-2 is distributed throughout the apical cortex

To examine the actomyosin architecture driving apical constriction of Ea and Ep, we first assessed the localization of non-muscle myosin II using a strain with NMY-2 endogenously tagged with mNeonGreen (mNG) at its N-terminus (Dickinson et al., 2015). The mNG::NMY-2 strain is fully viable (Dickinson et al., 2015; Table S3), despite NMY-2 being an essential protein (Guo and Kemphues, 1996), indicating that N-terminally tagged NMY-2 is functional. mNG::NMY-2 is enriched apically in apically constricting cells in this strain (Marston et al., 2016; Slabodnick et al., 2022 *Preprint*), consistent with previous observations of a fluorescently labeled transgene (Roh-Johnson et al., 2012) and matching native protein distribution based on immunofluorescence (Nance and Priess, 2002). Therefore, we used this strain to enable quantification of NMY-2 localization over time, in live embryos, to look for any enrichment in parts of the medioapical domain and throughout the process of apical constriction. For NMY-2 and the other proteins whose distribution we quantified in this study, we collected time-lapse movies of 10 or more embryos, time-aligned them using the birth of the neighboring MSxx cells as a reference point, and normalized cell lengths. We then measured intensity profiles along the anterior–posterior and left–right axes of both Ea and Ep using maximum intensity Z-projections of their apical surfaces (see Materials and methods for additional details). Given the punctate localization of mNG-NMY-2 throughout the apical cortex of Ea and Ep, we aggregated the intensity data from all samples (Fig. 2 and Fig. S1 A). The normalized intensity plots

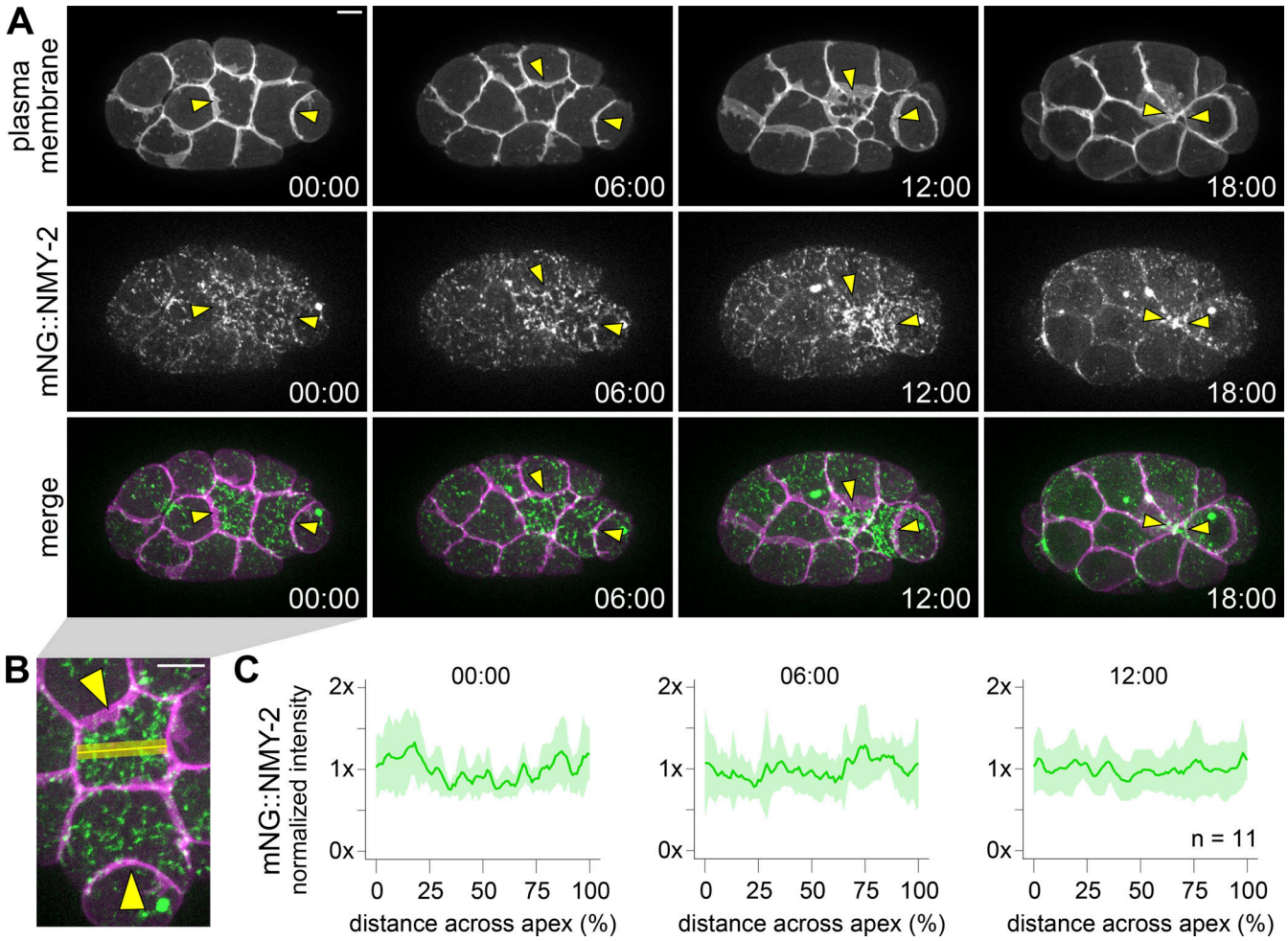

Figure 2. **NMY-2 exhibits punctate localization distributed throughout the apical cortex during apical constriction. (A)** Micrographs from a time-lapse movie depicting dynamic localization of mNG::NMY-2 over time from a ventral view. NMY-2 is covisualized with mScarlet-I::PH, which labels the plasma membrane. Yellow arrowheads point to Ea and Ep cells. **(B)** An enlarged micrograph from panel A to demonstrate how line scan (yellow line) measurements were collected. **(C)** Plots depicting fluorescence intensity of mNG::NMY-2, normalized to the mean intensity, along the left–right axis of Ea (n = 11 embryos). Solid lines indicate the mean, and shaded areas indicate the mean ± SD. Time represents minutes following the birth of the neighboring MSxx cells. Scale bars: 5 µm.

showed no clear trend pointing to the enrichment of mNG::NMY-2 in the center of the apex of Ea and Ep (Fig. 2 C and Fig. S1 A). We conclude that non-muscle myosin II punctae are broadly distributed throughout the apical cortex of Ea and Ep, throughout the process of apical constriction.

The myosin-activating kinase MRCK-1 is distributed throughout the apical cortex with slight apicolateral enrichment

While non-muscle myosin II did not exhibit enrichment at the center of the apex, it is possible that myosin activation is enriched in this region. To test this, we examined the myotonic dystrophy-related, Cdc42-binding kinase homolog MRCK-1. MRCKs are Cdc42 effectors that can activate myosin II motors by phosphorylating their regulatory light chains, performing a role similar to the Rho effector Rho kinase (Zhao and Manser, 2015). MRCK-1 is necessary for activating myosin during Ea/Ep internalization in *C. elegans* (Marston et al., 2016). We visualized and measured localization of MRCK-1 using a YPET-tagged allele (Marston et al., 2016). We found that MRCK-1 exhibits slight enrichment apicolaterally at sites of cell–cell contacts (Fig. 3, A and B). However, we did not find any evidence of enrichment in the center of the apex of Ea/Ep. We conclude that the myosin-activating kinase MRCK-1 is broadly distributed throughout the apical cell cortex and not enriched near the center of the apex.

CAP-1, a barbed-end capping protein, is enriched at apicolateral junctions

Next, we sought to examine the actin architecture of the apical cortex during Ea/Ep internalization. In the *Drosophila* ventral furrow, actin filaments were observed to be organized radially with enrichment of barbed-end markers at apicolateral junctions and enrichment of a pointed-end marker in the center of the cell apex (Coravos and Martin, 2016). To visualize actin filament polarity, we endogenously tagged actin filament capping proteins. We used the gene ontology search function on WormBase (Harris et al., 2020) to identify proteins with actin filament capping functions encoded within the *C. elegans*

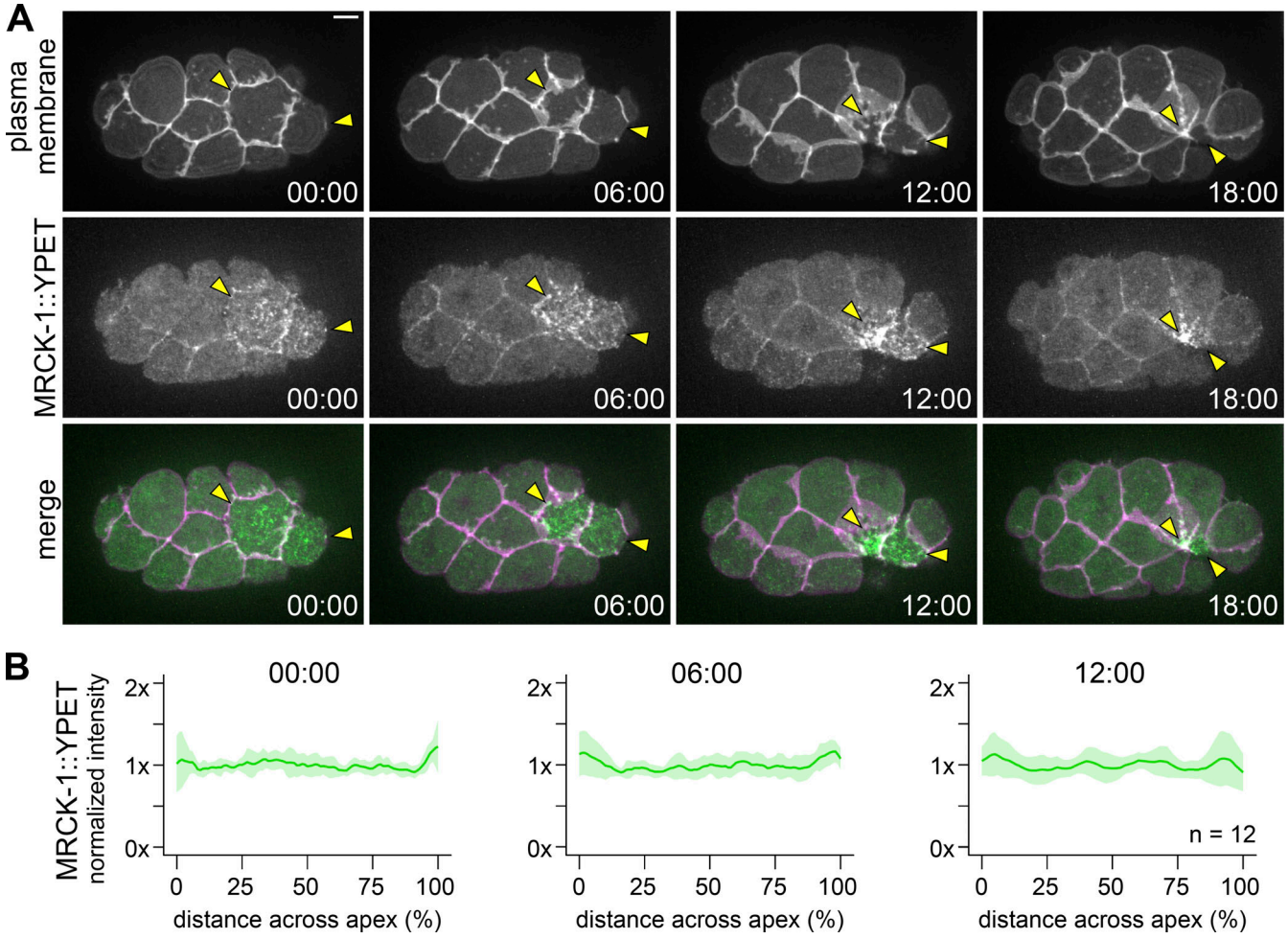

Figure 3. **MRCK-1 exhibits slight enrichment at cell–cell borders and not at the center of the apex. (A)** Micrographs from a time-lapse movie depicting dynamic localization of MRCK-1::YPET over time from a ventral view. MRCK-1 is covisualized with mScarlet-I::PH, which labels the plasma membrane. Yellow arrowheads point to Ea and Ep. **(B)** Plots depicting normalized fluorescence intensity of MRCK-1::YPET along the left–right axis of Ea (n = 12 embryos). Solid lines indicate the mean and shaded areas indicate the mean ± SD. Time represents minutes following the birth of the neighboring MSxx cells. Scale bar: 5 µm.

genome, and we referenced single-cell RNA-sequencing database (Differential Expression Gene Explorer; Tintori et al., 2016; Tintori et al., 2020) to predict which are expressed at detectable levels in the embryo at the time of Ea/Ep internalization.

Using CRISPR/Cas9 genome engineering, we tagged three genes annotated as encoding proteins with barbed-end actin filament capping functions: the α subunit of the capping protein homolog *cap-1* (Waddle et al., 1993), the receptor tyrosine kinase substrate *eps-8* (Croce et al., 2004), and the gelsolin-like protein *fli-1* (Campbell et al., 1993). The *eps-8* locus encodes 12 different isoforms due to a combination of splice variants and multiple transcriptional start sites. We tagged *eps-8* at its C-terminus with mNG as this would label all but one isoform, EPS-8B, whose essential role in the intestine has already been excluded (Croce et al., 2004; Fig. S2 A). Our sequence-confirmed EPS-8::mNG allele was expressed at levels below the detectable threshold on our imaging system, appearing similar to unlabeled, wild-type N2 control embryos at the time of Ea/Ep internalization (Fig. S2 B). We tagged the C-terminus of *fli-1* and the N-terminus of *cap-1* with mNG (Fig. S2, C–F). Both were detectable, but the *cap-1* strain was considerably brighter, consistent with predictions based on mRNA levels (Tintori et al., 2016; Tintori et al., 2020); thus, we proceeded with *cap-1* for quantitative analyses. We retagged CAP-1 with a red fluorescent protein, mScarlet-I, to pair it with mNG-tagged pointed-end capping protein, described below (Fig. 4, A and C); the double-labeled strain was fully viable (Table S3).

Quantification of mScarlet-I::CAP-1 localization revealed enrichment at cell–cell contacts, with significant enrichment observed at the boundary of the Ep and P_4 cells (Fig. 4, D and E, and Fig. S1 C). CAP-1 near the edges of apical domains might be part of the contractile networks or part of F-actin–rich protrusions that form near apical junctions of embryonic cells (Pohl and Bao, 2010). In either case, this result is similar to that observed by Coravos and Martin (2016) in the *Drosophila* ventral furrow, with barbed-end capping protein showing some enrichment near junctions. However, to determine if actin filaments exhibit similar radial polarity as in *Drosophila* ventral furrow cells, we also needed to examine the localization of the pointed ends.

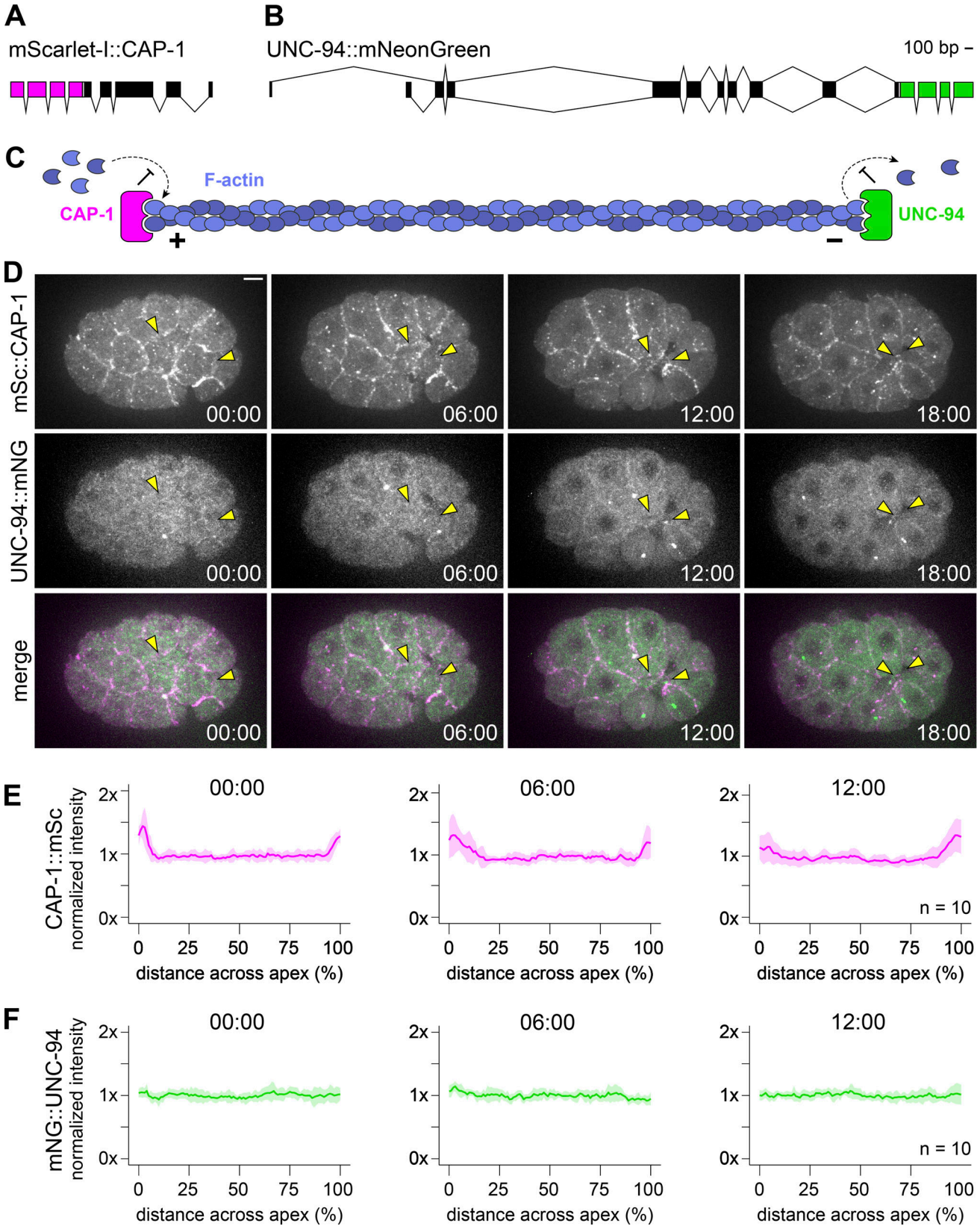

Figure 4. **Localization of barbed- and pointed-end capping proteins CAP-1 and UNC-94. (A)** Schematic of the endogenous *cap-1* locus tagged with mScarlet-I at its N-terminus. **(B)** Schematic of the endogenous *unc-94* locus tagged with mNeonGreenG at its C-terminus. **(C)** Cartoon of CAP-1 (magenta) and UNC-94 (green) performing their actin filament (blue) capping functions on the barbed (+) and pointed (−) ends, respectively. **(D)** Micrographs from a time-lapse movie depicting localization of mScarlet-I::CAP-1 and UNC-94::mNG over time from a ventral view. Yellow arrowheads point to Ea and Ep. **(E and F)** Plots depicting normalized fluorescence intensity of mScarlet-I::CAP-1 (E) and UNC-94::mNG (F) along the left–right axis of Ea (n = 10 embryos). Solid lines indicate the mean and shaded areas indicate the mean ± SD. Time represents minutes following the birth of the neighboring MSxx cells. Scale bar: 5 µm.

UNC-94, a pointed-end capping protein, is distributed throughout the apical cortex

To identify *C. elegans* genes encoding proteins with pointed-end actin filament capping functions, we again turned to the gene ontology search function on WormBase (Harris et al., 2020). Two pointed-end actin filament capping proteins were identified as homologous to tropomodulin: TMD-2 and UNC-94. According to the RNA-sequencing dataset available on Differential Expression Gene Explorer (Tintori et al., 2016; Tintori et al., 2020), *tmd-2* is not expressed in the internalizing Ea/Ep cells nor their precursors (E and EMS). Therefore, we focused our efforts on assessing UNC-94 localization.

The *unc-94* locus encodes two isoforms, UNC-94A and UNC-94B, with unique transcriptional start sites. We tagged each isoform independently using N-terminal mNG fusions and both isoforms together using a C-terminal mNG fusion (Fig. S3 A). While the mNG::UNC-94A allele was brighter than the mNG::UNC-94B allele, they exhibited similar patterns of localization (Fig. S3, B and C). Therefore, we utilized the C-terminally tagged version to examine the total distribution of both isoforms. We generated a strain with UNC-94 endogenously tagged in this way together with mTurquoise2::CAP-1, as well as a single-copy transgene expressing an F-actin marker, LifeAct::mScarlet-I (Fig. S3 E). This strain showed where each protein localized, but bleed-through between channels limited its utility for quantification. Therefore, we quantified UNC-94::mNG localization instead in a strain with only CAP-1 also labeled. Quantification of UNC-94::mNG localization revealed no evidence of enrichment in any part of the cell apex (Fig. 4, D and F). This also held true for experiments in which we increased laser power and exposure time without concern for photobleaching to collect single, static images (Fig. S3 D). Taken together, our results examining barbed-end and pointed-end capping protein localization suggest that actin filaments are not organized in a radial sarcomere-like orientation in Ea and Ep during apical constriction and instead are of mixed polarity.

Concluding remarks and future perspectives

Our data suggest that the medioapical actomyosin network that drives apical constriction in Ea/Ep cells during *C. elegans* gastrulation is diffusely organized, with non-muscle myosin II (NMY-2) and MRCK-1 distributed sparsely throughout the apical cortex (Fig. 5). While we did observe apicolateral enrichment of the barbed-end capping protein CAP-1, its pointed-end counterpart UNC-94 did not exhibit any central enrichment. These observations are in stark contrast to actomyosin networks observed in *Drosophila* ventral furrow cells, where a radial sarcomere-like organization was found, and where there is evidence that enrichment of a myosin-activating kinase in the center of the cell apex is essential for apical constriction (Coravos and Martin, 2016). Taken together, the observations made by us and others highlight that diverse strategies of actomyosin organization are used in animal cells to accomplish apical constriction.

A cellular architecture with radially polarized actin filaments and centrally enriched myosin and myosin activator, as seen in *Drosophila*, is an organization for which contraction of the actomyosin network is a readily expected outcome of myosin activation. Actomyosin networks with randomly oriented actin filaments might be expected to generate balanced compressive and tensile stresses, yet such networks can contract in vitro, owing at least in part to the buckling and severing of compressed actin filaments breaking this balance (Murrell and Gardel, 2012). Given the cortical organization that we found, we speculate that such buckling and severing could make important contributions to the forces driving apical constriction in *C. elegans*, and perhaps in other systems.

There is growing evidence that apically constricting cells rely less on the circumferential belts and more on medioapical actomyosin than initially expected (Davidson, 2012). For cells with flat or concave apical surfaces, purse string–like contraction of circumferential belts might effectively shrink apical domains, whereas, for cells with bulged apical surfaces, purse string–like contraction of circumferential belts might be expected to pinch cells in two. In our own sampling of the literature, summarized in Table S1 and Fig. 5, we noticed apparent examples of actomyosin networks being organized medioapically in addition to circumferentially in multiple systems: *Xenopus* (Baldwin et al., 2022 *Preprint*; Matsuda et al., 2022), chick (Nishimura and Takeichi, 2008; Nishimura et al., 2012; Sai et al., 2014), mouse (Ebrahim et al., 2013; Lang et al., 2014; Sumigray et al., 2018; Francou et al., 2023), and the *Drosophila* salivary gland placode (Röper, 2012; Booth et al., 2014; Chung et al., 2017). It is possible that some cells and tissues use both medioapical and circumferential actomyosin networks to accomplish apical constriction. A circumferential network is not apparent in *C. elegans*, although it is possible that a weak one exists, using only a low level of myosin. As a result, *C. elegans* gastrulation may provide a valuable model to dissect the dynamics and contributions of diffuse, medioapical actomyosin networks.

With methods for CRISPR and live-cell imaging advancing, future work with other organisms may allow for quantification of actomyosin architecture, as we have done here, and more cross-species comparisons. The use of endogenously tagged proteins can help avoid potential artifacts caused by overexpression in some systems, and live-cell imaging will enable the capture of protein distributions that may occur in only certain stages of apical constriction. Such information may make it possible to infer whether different actomyosin architectures are associated with other key aspects of morphogenesis, such as the internalization of a few cells at a time during *C. elegans* gastrulation versus the folding of large sheets of tissue during *Drosophila* ventral furrow formation.

Materials and methods

Strain maintenance

The strains used in this study are listed in Table S2. Animals were maintained on Nematode Growth Medium plates at 20°C under standard conditions (Brenner, 1974).

CRISPR-mediated genome engineering

The single-copy germline optimized LifeAct transgene was inserted into a neutral site on chromosome II (ttTi5605) using a

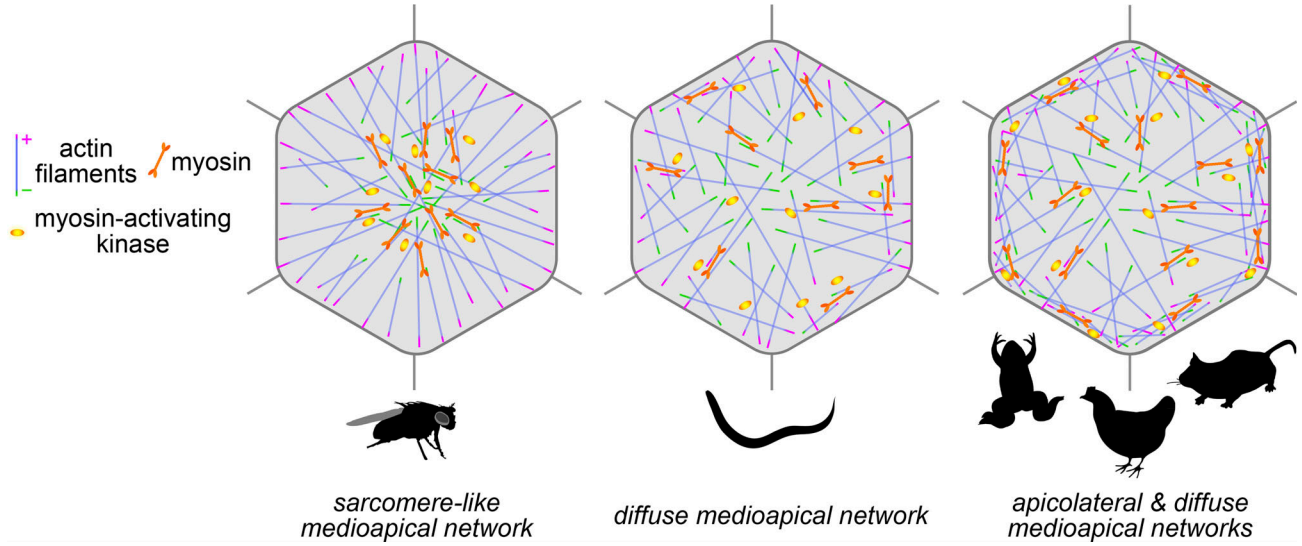

Figure 5. **Actomyosin architectures driving apical constriction in diverse biological contexts.** Illustrations depicting actin filament polarization and localization of myosin and myosin-activating kinase in the *Drosophila* ventral furrow, *C. elegans* gastrulation, and other contexts of apical constriction in *Xenopus*, chick, and mouse (see Table S1 for additional details).

repair template also containing a self-excising cassette with selectable markers to facilitate screening (Dickinson et al., 2015) paired with a plasmid encoding Cas9 and sgRNA (pDD122, #47550; AddGene). The new endogenously tagged strains presented in this work were generated through a previously described CRISPR/Cas9-mediated genome editing protocol (Ghanta and Mello, 2020). Briefly, 5 µl of 0.4 µg/µl tracrRNA and 2.8 µl of 0.4 µg/µl crRNA were added to 0.5 µl of 10 µg/µl Cas9 protein (all reagents from IDT). The mixture was incubated at 37°C for 15 min. 5 µl of 100 ng/µl double-stranded DNA donor, consisting of codon-optimized mNG (amplified from pDD268, #132523; AddGene), mScarlet-I (amplified from pMS050, #91826; AddGene), or mTurquoise2 (amplified from pDD315, AddGene #132523) with 35 bp homology arms, was melted and cooled before being added to the mixture. 1.6 µl of 500 ng/µl pRF4 (*rol-6(su1006)*) plasmid was also added as a coinjection marker. Nuclease-free water was used to bring the final volume to 20 µl. The mixture was then centrifuged at 14,000 rpm for 2 min. 17 µl of the mixture was transferred to a fresh tube and kept on ice during the injection. Heterozygous mutants were then selected by genotyping F1 non-rollers or examining F1 under a Zeiss Axiozoom V16 stereo microscope. Homozygotes were sequenced to confirm the edits. crRNAs and homology arms sequences can be found in Table S4. Characterization of tagged alleles was performed by comparing with known expression and localization patterns available on WormBase (Harris et al., 2020) and by measuring embryo hatching rates (Table S3). Briefly, L4-stage animals from each strain were left on 6–11 plates for 24 h. The worms were then removed and the embryos laid on each plate were counted. The embryos were examined again after 24 h to determine the percentage that had hatched.

Live-cell imaging

Embryos were dissected from gravid adults and mounted on slides in *C. elegans* egg buffer and sealed with 1:1:1 mixture by weight of vaseline, lanolin, and paraffin. For ventral mounts, glass beads ~23 µm in diameter (Whitehouse Scientific Monodisperse Standards, MS0023) and clay feet were used to separate the slide and coverslip. For lateral mounts, 2.5% agar pads were used. The *mrck-1*::YPET strain was imaged with a Hamamatsu C11440-22CU ORCA Flash 4.0 sCMOS camera mounted on a Nikon Eclipse Ti inverted confocal microscope with Yokogawa QLC100/CSU10 spinning-disk scan head. All other strains were imaged with a Hamamatsu ORCA QUEST qCMOS camera mounted on a Nikon Eclipse Ti inverted confocal microscope with a Yokogawa CSU-X1 spinning-disk scan head. All micrographs were collected at room temperature using a 60× 1.4 NA oil immersion lens and a 1.5× magnifier paired with 514 and 561 nm coherent lasers. Z-stacks through the ventral surface of the embryo with a step size of 0.5–1 µm were collected every 2–3 min.

Image quantification

ImageJ/FIJI was used for data quantification (Schindelin et al., 2012). Intensity profiles along left–right and anterior–posterior axes were collected from maximum intensity Z-projections of the ventral surface using a line width of ~1.5 µm. The distance along the axis was normalized to adjust for variability in cell apex size/shape among embryos and subjected to linear interpolation sampled at each integer. The intensity was normalized to the mean. Movies were time-aligned using the timing of MSxx cell birth. The relative intensity of the mNG-tagged *unc-94* alleles was quantified from maximum intensity Z-projections of embryos at the time of MSxx cell birth. Intensity was measured by drawing a region of interest around the embryo and measuring the mean gray value, and then manually subtracting the mean gray value of a background region to account for camera noise.

Data visualization

Representative micrographs from time-lapse movies were processed in ImageJ/FIJI (Schindelin et al., 2012). Intensity profiles

were plotted using the ggplot2 package in R (Wickham, 2016). Schematics of gene loci were generated using the Exon–Intron Graphic Maker (http://wormweb.org/exonintron). Animal silhouettes were retrieved from Adobe Stock and PhyloPic (http://phylopic.org/). Figures were assembled in Adobe Illustrator.

Online supplemental material

Fig. S1 shows the quantification of endogenously tagged NMY-2, MRCK-1, CAP-1, and UNC-94 intensity profiles in Ea and Ep. Fig. S2 shows micrographs of endogenously tagged barbed-end actin filament proteins EPS-8, FLI-1, and CAP-1. Fig. S3 compares the expression and localization of endogenously tagged UNC-94 isoforms and shows covisualization of UNC-94 with CAP-1 and actin filaments. Table S1 summarizes what is known about actomyosin organization present during apical constriction in diverse organisms and biological contexts, according to existing literature. Table S2 lists the strains used in this study. Table S3 reports embryo hatching rates. Table S4 provides the sequences used for CRISPR/Cas9 genome editing.

Data availability

The data are available from the corresponding author upon reasonable request.

Acknowledgments

We thank members of the Goldstein lab, Ed Munro, Amy Shaub Maddox, and Stephanie Gupton for helpful feedback, discussion, and critical reading of the manuscript. We also thank Emily Bowie for her contributions toward generating the strain to visualize actin localization.

This work was supported by a Maximizing Investigators' Research Award (R35GM134838 to B. Goldstein) from the National Institutes of Health.

Author contributions: P. Zhang and B. Goldstein conceptualized the study. P. Zhang and T.N. Medwig-Kinney designed the methodology and performed the investigation. P. Zhang led project administration, data curation, and validation. T.N. Medwig-Kinney performed the formal analyses, provided resources, and data visualization. B. Goldstein acquired funding and supervised the study. T.N. Medwig-Kinney and P. Zhang wrote the original draft of the manuscript, and all authors reviewed and edited the manuscript.

Disclosures: The authors declare no competing interests exist.

Submitted: 24 February 2023
Revised: 24 May 2023
Accepted: 6 June 2023

References

Baker, P.C., and T.E. Schroeder. 1967. Cytoplasmic filaments and morphogenetic movement in the amphibian neural tube. *Dev. Biol.* 15:432–450. https://doi.org/10.1016/0012-1606(67)90036-X

Baldwin, A.T., I.K. Popov, R. Keller, J.B. Wallingford, and C. Chang. 2022. The RhoGEF protein Plekhg5 regulates medioapical actomyosin dynamics of apical constriction during Xenopus gastrulation. *bioRxiv*. (Preprint posted September 02, 2022). https://doi.org/10.1101/2022.08.31.506049

Booth, A.J.R., G.B. Blanchard, R.J. Adams, and K. Röper. 2014. A dynamic microtubule cytoskeleton directs medial actomyosin function during tube formation. *Dev. Cell*. 29:562–576. https://doi.org/10.1016/j.devcel.2014.03.023

Brenner, S. 1974. The genetics of Caenorhabditis elegans. *Genetics*. 77:71–94. https://doi.org/10.1093/genetics/77.1.71

Burnside, B. 1973. Microtubules and microfilaments in amphibian neurulation. *Am. Zool.* 13:989–1006. https://doi.org/10.1093/icb/13.4.989

Campbell, H.D., T. Schimansky, C. Claudianos, N. Ozsarac, A.B. Kasprzak, J.N. Cotsell, I.G. Young, H.G. de Couet, and G.L. Miklos. 1993. The *Drosophila* melanogaster flightless-I gene involved in gastrulation and muscle degeneration encodes gelsolin-like and leucine-rich repeat domains and is conserved in Caenorhabditis elegans and humans. *Proc. Natl. Acad. Sci. USA*. 90:11386–11390. https://doi.org/10.1073/pnas.90.23.11386

Chung, S., S. Kim, and D.J. Andrew. 2017. Uncoupling apical constriction from tissue invagination. *Elife*. 6:e22235. https://doi.org/10.7554/eLife.22235

Coravos, J.S., and A.C. Martin. 2016. Apical sarcomere-like actomyosin contracts nonmuscle *Drosophila* epithelial cells. *Dev. Cell*. 39:346–358. https://doi.org/10.1016/j.devcel.2016.09.023

Croce, A., G. Cassata, A. Disanza, M.C. Gagliani, C. Tacchetti, M.G. Malabarba, M.-F. Carlier, G. Scita, R. Baumeister, and P.P. Di Fiore. 2004. A novel actin barbed-end-capping activity in EPS-8 regulates apical morphogenesis in intestinal cells of Caenorhabditis elegans. *Nat. Cell Biol.* 6:1173–1179. https://doi.org/10.1038/ncb1198

Davidson, L.A. 2012. No strings attached: New insights into epithelial morphogenesis. *BMC Biol.* 10:105. https://doi.org/10.1186/1741-7007-10-105

Dickinson, D.J., A.M. Pani, J.K. Heppert, C.D. Higgins, and B. Goldstein. 2015. Streamlined genome engineering with a self-excising drug selection cassette. *Genetics*. 200:1035–1049. https://doi.org/10.1534/genetics.115.178335

Ebrahim, S., T. Fujita, B.A. Millis, E. Kozin, X. Ma, S. Kawamoto, M.A. Baird, M. Davidson, S. Yonemura, Y. Hisa, et al. 2013. NMII forms a contractile transcellular sarcomeric network to regulate apical cell junctions and tissue geometry. *Curr. Biol.* 23:731–736. https://doi.org/10.1016/j.cub.2013.03.039

Francou, A., K.V. Anderson, and A.-K. Hadjantonakis. 2023. A ratchet-like apical constriction drives cell ingression during the mouse gastrulation EMT. *Elife*. 12:e84019. https://doi.org/10.7554/eLife.84019

Ghanta, K.S., and C.C. Mello. 2020. Melting dsDNA donor molecules greatly improves precision genome editing in Caenorhabditis elegans. *Genetics*. 216:643–650. https://doi.org/10.1534/genetics.120.303564

Goldstein, B., and J. Nance. 2020. Caenorhabditis elegans gastrulation: A model for understanding how cells polarize, change shape, and journey toward the center of an embryo. *Genetics*. 214:265–277. https://doi.org/10.1534/genetics.119.300240

Guo, S., and K.J. Kemphues. 1996. A non-muscle myosin required for embryonic polarity in *Caenorhabditis elegans*. *Nature*. 382:455–458. https://doi.org/10.1038/382455a0

Harris, T.W., V. Arnaboldi, S. Cain, J. Chan, W.J. Chen, J. Cho, P. Davis, S. Gao, C.A. Grove, R. Kishore, et al. 2020. WormBase: A modern model organism information resource. *Nucleic Acids Res.* 48:D762–D767. https://doi.org/10.1093/nar/gkz920

Lang, R.A., K. Herman, A.B. Reynolds, J.D. Hildebrand, and T.F. Plageman Jr. 2014. p120-catenin-dependent junctional recruitment of Shroom3 is required for apical constriction during lens pit morphogenesis. *Development*. 141:3177–3187. https://doi.org/10.1242/dev.107433

Marston, D.J., C.D. Higgins, K.A. Peters, T.D. Cupp, D.J. Dickinson, A.M. Pani, R.P. Moore, A.H. Cox, D.P. Kiehart, and B. Goldstein. 2016. MRCK-1 drives apical constriction in C. elegans by linking developmental patterning to force generation. *Curr. Biol.* 26:2079–2089. https://doi.org/10.1016/j.cub.2016.06.010

Martin, A.C., and B. Goldstein. 2014. Apical constriction: Themes and variations on a cellular mechanism driving morphogenesis. *Development*. 141:1987–1998. https://doi.org/10.1242/dev.102228

Martin, A.C., M. Kaschube, and E.F. Wieschaus. 2009. Pulsed contractions of an actin-myosin network drive apical constriction. *Nature*. 457:495–499. https://doi.org/10.1038/nature07522

Mason, F.M., M. Tworoger, and A.C. Martin. 2013. Apical domain polarization localizes actin-myosin activity to drive ratchet-like apical constriction. *Nat. Cell Biol.* 15:926–936. https://doi.org/10.1038/ncb2796

Matsuda, M., C.-W. Chu, and S.Y. Sokol. 2022. Lmo7 recruits myosin II heavy chain to regulate actomyosin contractility and apical domain size in Xenopus ectoderm. *Development*. 149:dev200236. https://doi.org/10.1242/dev.200236

Murrell, M.P., and M.L. Gardel. 2012. F-actin buckling coordinates contractility and severing in a biomimetic actomyosin cortex. *Proc. Natl. Acad. Sci. USA*. 109:20820–20825. https://doi.org/10.1073/pnas.1214753109

Nance, J., and J.R. Priess. 2002. Cell polarity and gastrulation in C. elegans. *Development*. 129:387–397. https://doi.org/10.1242/dev.129.2.387

Nishimura, T., H. Honda, and M. Takeichi. 2012. Planar cell polarity links axes of spatial dynamics in neural-tube closure. *Cell*. 149:1084–1097. https://doi.org/10.1016/j.cell.2012.04.021

Nishimura, T., and M. Takeichi. 2008. Shroom3-mediated recruitment of Rho kinases to the apical cell junctions regulates epithelial and neuroepithelial planar remodeling. *Development*. 135:1493–1502. https://doi.org/10.1242/dev.019646

Pohl, C., and Z. Bao. 2010. Chiral forces organize left-right patterning in C. elegans by uncoupling midline and anteroposterior axis. *Dev. Cell*. 19:402–412. https://doi.org/10.1016/j.devcel.2010.08.014

Roh-Johnson, M., G. Shemer, C.D. Higgins, J.H. McClellan, A.D. Werts, U.S. Tulu, L. Gao, E. Betzig, D.P. Kiehart, and B. Goldstein. 2012. Triggering a cell shape change by exploiting preexisting actomyosin contractions. *Science*. 335:1232–1235. https://doi.org/10.1126/science.1217869

Röper, K.. 2012. Anisotropy of Crumbs and aPKC drives myosin cable assembly during tube formation. *Dev. Cell*. 23:939–953. https://doi.org/10.1016/j.devcel.2012.09.013

Sai, X., S. Yonemura, and R.K. Ladher. 2014. Junctionally restricted RhoA activity is necessary for apical constriction during phase 2 inner ear placode invagination. *Dev. Biol.* 394:206–216. https://doi.org/10.1016/j.ydbio.2014.08.022

Sawyer, J.M., J.R. Harrell, G. Shemer, J. Sullivan-Brown, M. Roh-Johnson, and B. Goldstein. 2010. Apical constriction: A cell shape change that can drive morphogenesis. *Dev. Biol.* 341:5–19. https://doi.org/10.1016/j.ydbio.2009.09.009

Schindelin, J., I. Arganda-Carreras, E. Frise, V. Kaynig, M. Longair, T. Pietzsch, S. Preibisch, C. Rueden, S. Saalfeld, B. Schmid, et al. 2012. Fiji: An open-source platform for biological-image analysis. *Nat. Methods*. 9:676–682. https://doi.org/10.1038/nmeth.2019

Slabodnick, M.M., S.C. Tintori, M. Prakash, and C.D. Higgins. 2022. Afadin and zyxin contribute to coupling between cell junctions and contractile actomyosin networks during apical constriction. *bioRxiv*. (Preprint posted July 04, 2022). https://doi.org/10.1101/2022.07.04.498649

Sumigray, K.D., M. Terwilliger, and T. Lechler. 2018. Morphogenesis and compartmentalization of the intestinal crypt. *Dev. Cell*. 45:183–197.e5. https://doi.org/10.1016/j.devcel.2018.03.024

Tintori, S.C., P. Golden, and B. Goldstein. 2020. Differential expression gene explorer (DrEdGE): A tool for generating interactive online visualizations of gene expression datasets. *Bioinformatics*. 36:2581–2583. https://doi.org/10.1093/bioinformatics/btz972

Tintori, S.C., E. Osborne Nishimura, P. Golden, J.D. Lieb, and B. Goldstein. 2016. A transcriptional lineage of the early C. elegans embryo. *Dev. Cell*. 38:430–444. https://doi.org/10.1016/j.devcel.2016.07.025

Waddle, J.A., J.A. Cooper, and R.H. Waterston. 1993. The α and β subunits of nematode actin capping protein function in yeast. *Mol. Biol. Cell*. 4:907–917. https://doi.org/10.1091/mbc.4.9.907

Wickham, H. 2016. ggplot2: Elegant Graphics for Data Analysis. Second edition. Springer-Verlag, New York.

Zhao, Z., and E. Manser. 2015. Myotonic dystrophy kinase-related Cdc42-binding kinases (MRCK), the ROCK-like effectors of Cdc42 and Rac1. *Small GTPases*. 6:81–88. https://doi.org/10.1080/21541248.2014.1000699

Supplemental material

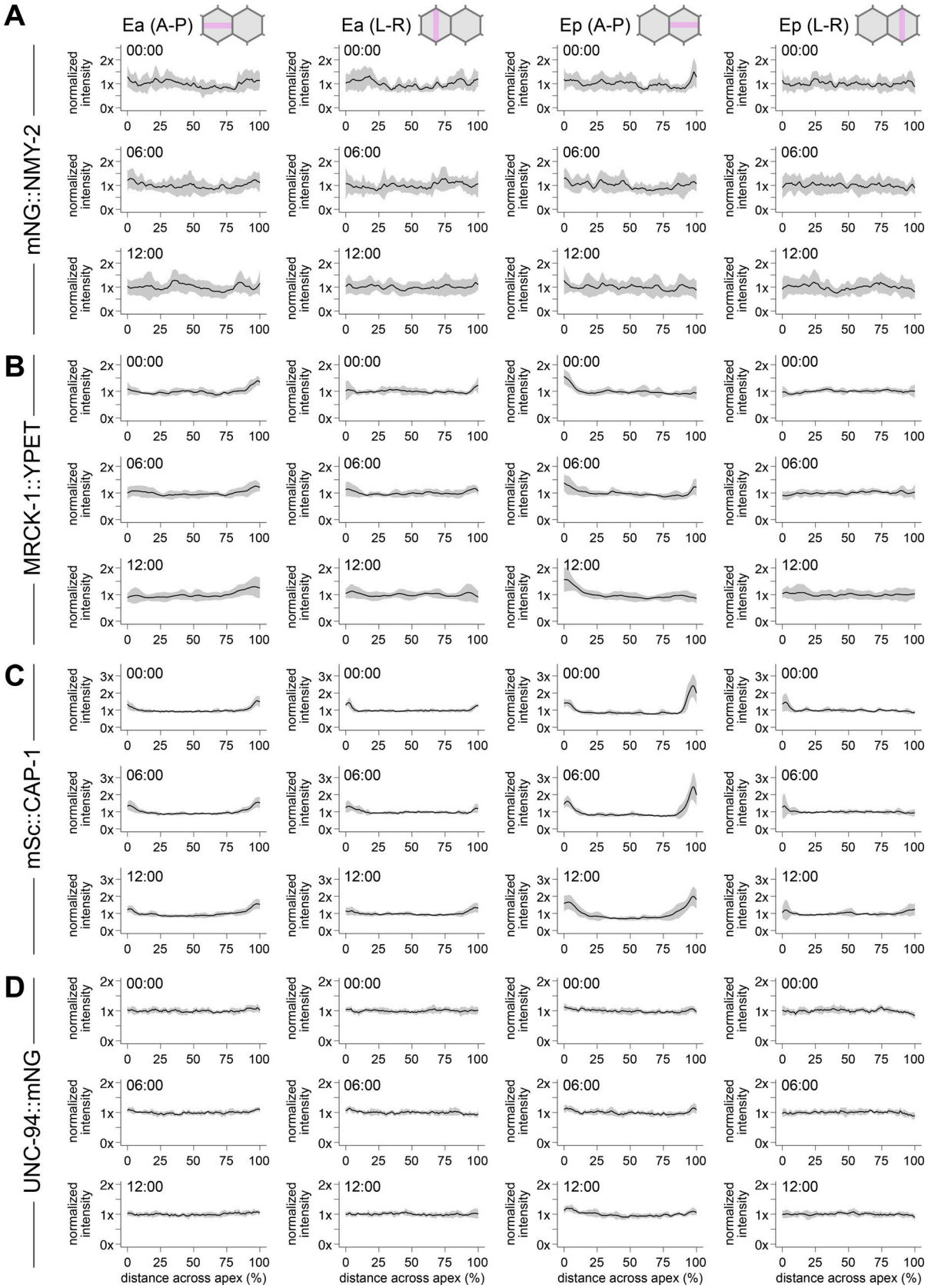

Figure S1. **Quantification of protein localization during apical constriction. (A–D)** Plots depicting normalized intensity of mNG::NMY-2 (A, *n* = 11 embryos), MRCK-1::YPET (B, *n* = 12 embryos), CAP-1::mScarlet-I (C, *n* = 10 embryos), and mNG::UNC-94 (D, *n* = 10 embryos) across the anterior–posterior (A-P) or left–right (L-R) axes of Ea and Ep. Time represents minutes following the birth of the MSxx cells. Solid lines indicate the mean and shaded areas indicate the mean ± SD.

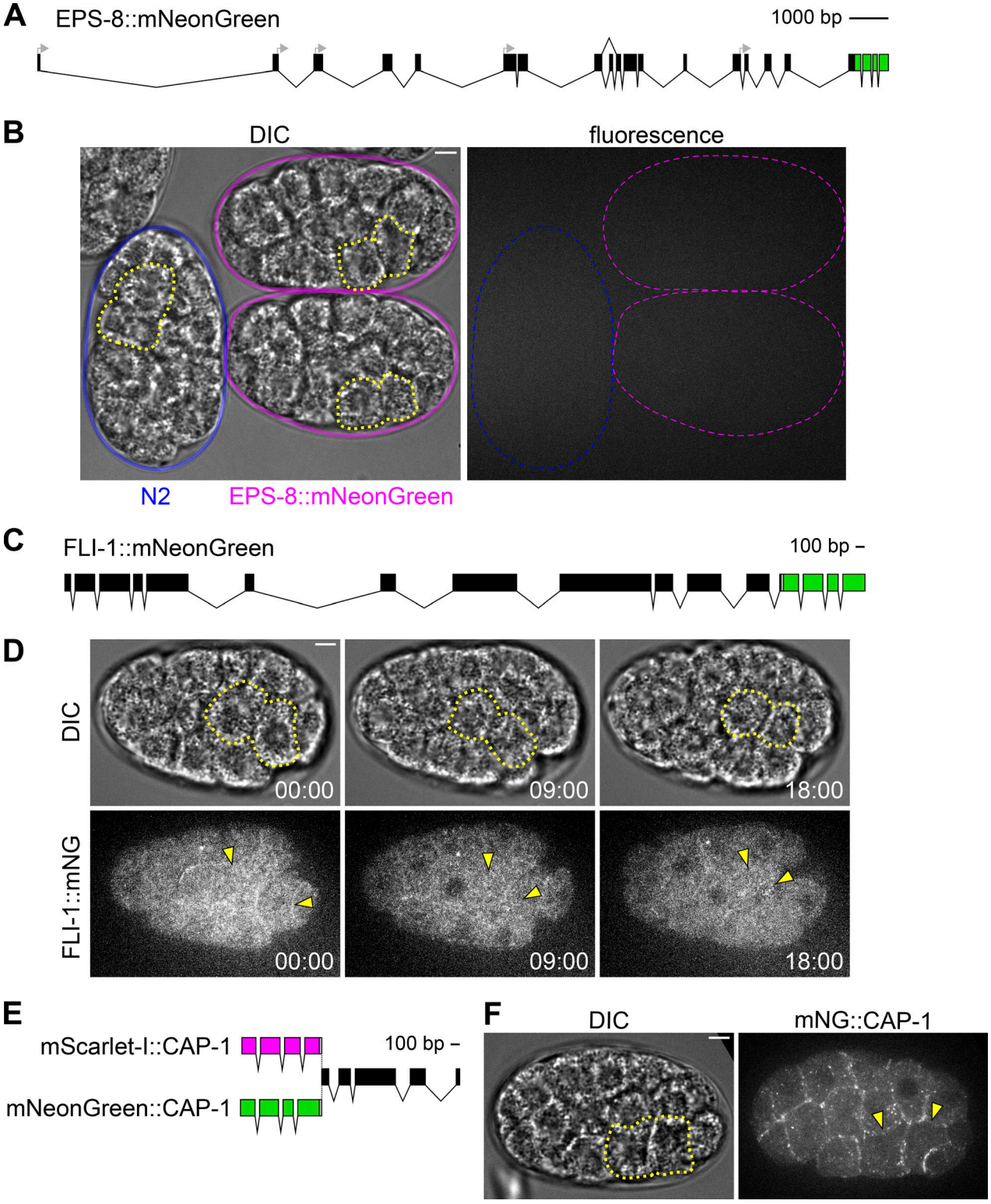

Figure S2. **Barbed-end actin filament proteins. (A)** Schematic of the endogenous *eps-8* locus tagged with mNG at its C-terminus. The start codons of the various isoforms are indicated with gray arrows. **(B)** Differential interference contrast (DIC, left) and fluorescence (right) micrographs of N2 control (blue) and EPS-8::mNG embryos (magenta) from a lateral view. **(C)** Schematic of the endogenous *fli-1* locus tagged with mNG at its C-terminus. **(D)** DIC (top) and fluorescence (bottom) micrographs from a time-lapse movie depicting localization of FLI-1::mNG over time from a ventral view. **(E)** Schematic of the endogenous *cap-1* locus tagged with either mScarlet-I or mNG at its N-terminus. **(F)** DIC (left) and fluorescence (right) micrographs depicting localization of mNG::CAP-1 from a ventral view. Ea and Ep are indicated with yellow dotted lines or arrowheads. Time represents minutes following the birth of the MSxx cells. Scale bars: 5 µm.

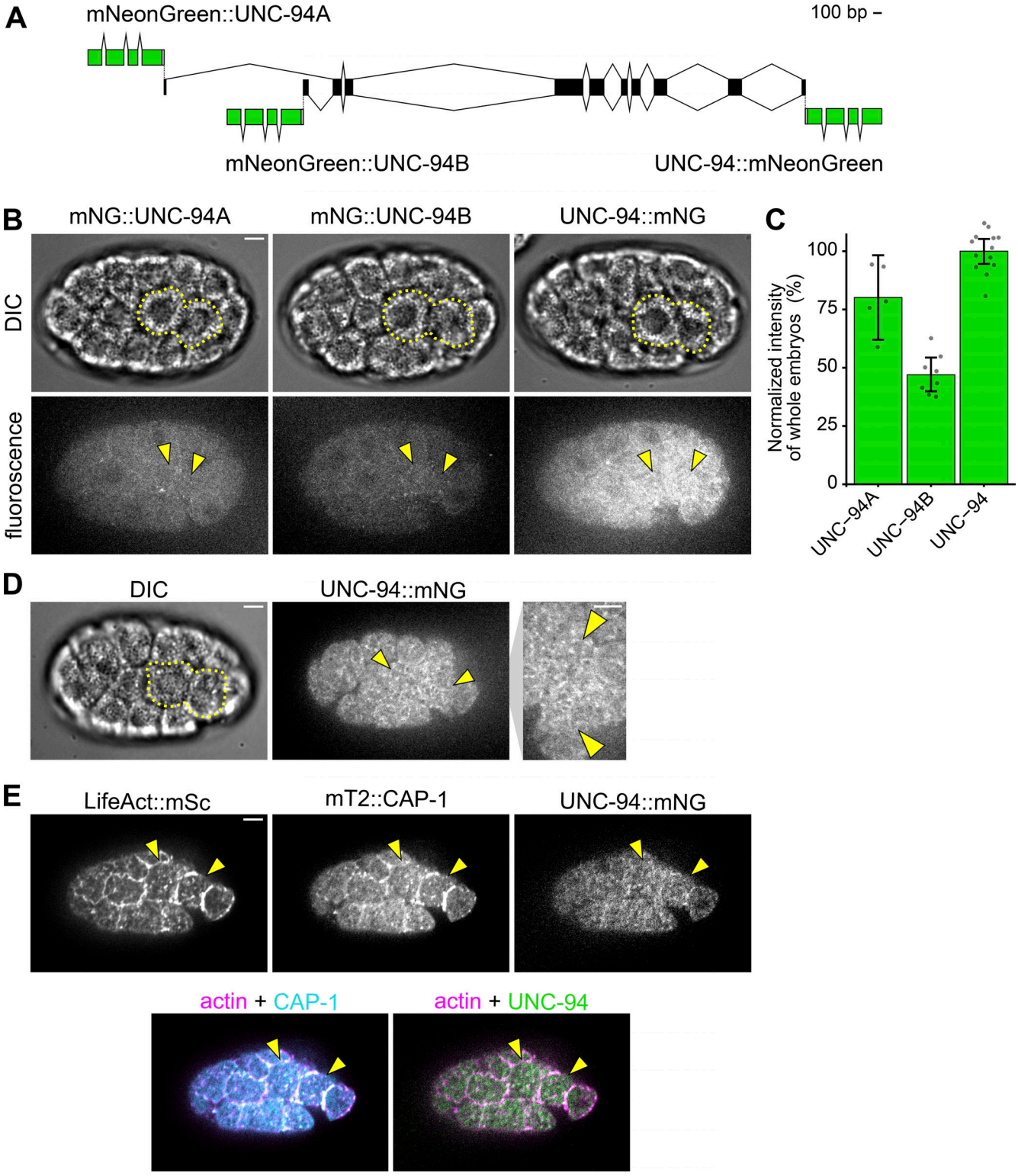

Figure S3. **Comparison of mNG-tagged UNC-94 isoforms and covisualization with CAP-1 and actin filaments. (A)** Schematic of the endogenous *unc-94* locus fused to mNG at its C-terminus (tagging both isoforms) or at the N-termini of the isoforms encoding either UNC-94A or UNC-94B. **(B)** Micrographs depicting expression and localization of UNC-94A::mNG, UNC-94B::mNG, and UNC-94::mNG from a ventral view. **(C)** Bar plot depicting relative intensity measurements of whole embryos with the UNC-94A::mNG, UNC-94B::mNG, and UNC-94::mNG alleles ($n \geq 5$ embryos). **(D)** Representative micrograph of UNC-94::mNG using imaging parameters optimized for static imaging. **(E)** Micrographs depicting localization of *mex-5p*::LifeAct::mScarlet-I, mTurquoise2::CAP-1, and UNC-94::mNG. Ea and Ep are indicated with yellow dotted lines or arrowheads. Error bars indicate SD. Scale bars: 5 µm.

Provided online are four tables. Table S1 shows the literature review. Table S2 shows the strains. Table S3 shows embryo hatching rates. Table S4 shows sequences of CRISPR/Cas9 reagents.